Forest Mapping and Classification at L band using POL-inSAR Optimal Coherence Set Statistics

Laurent Ferro-Famil[(1)], Florian Kugler[(2)], Eric Pottier[(1)] and Jong-Sen Lee[(3)]

[(1)]University of Rennes 1, IETR, Remote Sensing group, Rennes, France
[(2)]DLR, Microwave and Radar Institute, SAR technology department, Pol-inSAR group, Oberpfaffenhofen, Germany
[(3)]Remote Sensing Division, Naval Research Laboratory, Washington, DC, USA.

Abstract

This paper presents a new approach to classify forested areas from POL-inSAR data. The statistics of an optimal coherence set are derived to define a log-likelihood distance that can be used in iterative classification processes. This novel method is compared to an existing technique based on a POL-inSAR coherency matrix Wishart statistics. The invariance properties of optimal coherences may be used to overcome some limitations encountered with the Wishart approach. It is then shown that such an approach may be used to relyably classify forest stand biomass into broad categories.

1 Introduction

Recent studies [1] [2] have shown that over densely vegetated areas, POLSAR information suffers from a saturation effect and may not be sufficiently sensitive for classification purposes. POL-inSAR measurements can provide specific descriptors , closely related to forest stands physical properties [3], that can be efficiently integrated in a classification process. In a first part, a log-likelihood distance measure is derived from the joint statistical distribution of a Pol-inSAR optimized coherence set which is used in a second time to address both supervised and unsupervised classification types. The performance of the Wishart and the coherence based solutions are estimated and limitations are commented. Finally, an additional processing step is proposed to compensate the well known range dependence of volumetric interferometric decorrelation that may affect the classifier accuracy in the range direction.

2 POL-inSAR Data Statistics

2.1 POL-inSAR coherency matrix statistics

A scatterer POL-inSAR coherent response may be fully characterized using a 6-element complex target vector, $\mathbf{k}_6$, obtained by stacking the target vector from each POLSAR image. Over homogeneous areas, this vector follows a Gaussian circular complex pdf, $\mathcal{N}_c(\mathbf{0}, \mathbf{\Sigma}_6)$, with $\mathbf{\Sigma}_6 = E(\mathbf{k}_6\mathbf{k}_6^\dagger)$. The study of second order polarimetric properties can be achieved by sampling a coherency matrix $\mathbf{T}_6$ using n independent realizations of $\mathbf{k}_6$. The (6×6) sample coherency matrix $\mathbf{T}_6$ is hermitian definite positive and follows a complex Wishart pdf, $\mathcal{W}_c(n, \mathbf{\Sigma}_6)$. Its probability is defined as:

$$p(\mathbf{T}) = \frac{n^{qn}|\mathbf{T}|^{n-q}}{\tilde{\Gamma}(n)|\mathbf{\Sigma}|^n} \mathrm{e}^{tr(n\mathbf{\Sigma}^{-1}\mathbf{T})}, \mathbf{T} = \frac{1}{n}\sum_{i=1}^{n} \mathbf{k}\mathbf{k}^\dagger \qquad (1)$$

where $\tilde{\Gamma}(.)$ is the complex gamma function, q equals 6. A pseudo-distance can be derived from the log-likelihood of $\mathbf{T}_6$ with respect to a given average coherency matrix $\mathbf{\Sigma}_{6\_m}$:

$$d_W(\mathbf{T}_6, \mathbf{\Sigma}_{6\_m}) = |\mathbf{\Sigma}_{6\_m}| + tr(\mathbf{\Sigma}_{6\_m}^{-1}\mathbf{T}_6) \qquad (2)$$

A sample POL-inSAR coherency matrix, $\mathbf{T}_6$, may be represented under the following form :

$$\mathbf{T}_6 = \begin{bmatrix} \mathbf{T_{11}} & \mathbf{T_{12}} \\ \mathbf{T_{12}}^\dagger & \mathbf{T_{22}} \end{bmatrix} \text{ with } \mathbf{T}_{ij} = \frac{1}{n}\sum_{i=1}^{n} \mathbf{k}_i\mathbf{k}_j^\dagger \qquad (3)$$

where $\mathbf{T}_{ii}$ represents one of the separate POLSAR coherency matrix, and $\mathbf{T}_{12}$ the POL-INSAR correlation.

2.2 POL-inSAR optimal coherence statistics

2.2.1 POL-inSAR optimal coherence set

In [3], the authors use a generalization of the sample interferometric coherence to the POL-inSAR case expressed as :

$$\gamma(\mathbf{w}_1, \mathbf{w}_2) = \frac{\mathbf{w}_1^\dagger \mathbf{T}_{12} \mathbf{w}_2}{\sqrt{\mathbf{w}_1^\dagger \mathbf{T}_{11} \mathbf{w}_1 \, \mathbf{w}_2^\dagger \mathbf{T}_{22} \mathbf{w}_2}} \qquad (4)$$

where $\mathbf{w}_1$ and $\mathbf{w}_2$ represent polarimetric projection vectors. They also showed that particular projection vectors could maximize the modulus of the POL-inSAR coherence. This can be demonstrated very briefly by rewriting (4) as

$$\gamma(\tilde{\mathbf{w}}_1, \tilde{\mathbf{w}}_2) = \tilde{\mathbf{w}}_1^\dagger \mathbf{T}_{11}^{-\frac{1}{2}\dagger} \mathbf{T}_{12} \mathbf{T}_{22}^{-\frac{1}{2}} \tilde{\mathbf{w}}_2 = \tilde{\mathbf{w}}_1^\dagger \mathbf{\Pi} \tilde{\mathbf{w}}_2 \qquad (5)$$

where $\tilde{\mathbf{w}}_i$ is a unitary projection vector. The Cauchy-Schwarz inequality provides an upper bound for $|\gamma(\tilde{\mathbf{w}}_1, \tilde{\mathbf{w}}_2)|^2$:

$$|\gamma(\tilde{\mathbf{w}}_1, \tilde{\mathbf{w}}_2)|^2 \leq \tilde{\mathbf{w}}_i^\dagger \mathbf{\Pi}\mathbf{\Pi}^\dagger \tilde{\mathbf{w}}_i \quad i = 1, 2 \qquad (6)$$

The maximization of the quadratic form in (6) is a straightforward eigenvector problem. The optimum values are given by

$$|\gamma_{opt\,j}| = |r_j| \quad \text{and} \quad \mathbf{w}_{i\,opt\,j} = \mathbf{T}_{ii}^{-\frac{1}{2}} \mathbf{v}_j \qquad (7)$$

where $|r_j|^2$ stands for an eigenvalue of $\mathbf{\Pi\Pi}^\dagger$ and $\mathbf{v}_j$ its corresponding eigenvector. These developments show that the optimal coherence set is invariant by scaling or separate non-singular transformation of the polarimetric images

2.2.2 Optimal coherence set statistics

Due to the invariance properties mentioned above, the transformation relating a sample coherency matrix $\mathbf{T}_6$ having a $\mathcal{W}_c(n, \mathbf{\Sigma}_6)$ to $\tilde{\mathbf{T}}_6$ following a $\mathcal{W}_c(n, \tilde{\mathbf{\Sigma}}_6)$ with $\tilde{\mathbf{\Sigma}}_6$ given in (8) keeps the sample optimal coherence set unchanged.

$$\tilde{\mathbf{\Sigma}}_6 = \begin{bmatrix} \mathbf{I} & \mathbf{P} \\ \mathbf{P}^\dagger & \mathbf{I} \end{bmatrix}, \tilde{\mathbf{T}}_6 = \begin{bmatrix} \tilde{\mathbf{T}}_{\mathbf{11}} & \tilde{\mathbf{T}}_{\mathbf{12}} \\ \tilde{\mathbf{T}}_{\mathbf{12}}^\dagger & \tilde{\mathbf{T}}_{\mathbf{22}} \end{bmatrix} \quad (8)$$

where $\mathbf{P}$ represents the optimal coherence matrix of $\mathbf{\Sigma}_6$. The optimal coherence set of $\mathbf{T}_6$ verifies

$$|\tilde{\mathbf{T}}_{12}\tilde{\mathbf{T}}_{22}^{-1}\tilde{\mathbf{T}}_{12}^\dagger - |r_i|^2(\tilde{\mathbf{T}}_{11.2} + \tilde{\mathbf{T}}_{12}\tilde{\mathbf{T}}_{22}^{-1}\tilde{\mathbf{T}}_{12}^\dagger)| = 0 \quad (9)$$

with $\tilde{\mathbf{T}}_{11.2} = \tilde{\mathbf{T}}_{11} - \tilde{\mathbf{T}}_{12}\tilde{\mathbf{T}}_{22}^{-1}\tilde{\mathbf{T}}_{12}^\dagger$.
The joint pdf of $\tilde{\mathbf{T}}_{11.2}$, $\tilde{\mathbf{T}}_{12}$and $\tilde{\mathbf{T}}_{22}$ can be found in [4]. The term $\tilde{\mathbf{T}}_{11.2}$ is independent of the others and follows a $\mathcal{W}_c(n-q, \mathbf{I}-\mathbf{P}\mathbf{P}^\dagger)$ pdf, whereas conditional on $\tilde{\mathbf{T}}_{22}$, the distribution of $\tilde{\mathbf{T}}_{12}$ is $\mathcal{N}_c(\mathbf{P}\tilde{\mathbf{T}}_{12}, (\mathbf{I}-\mathbf{P}\mathbf{P}^\dagger)\otimes\mathbf{I})$. One may deduce from the last expression that the left hand term of (9) has a non-central Wishart distribution $\mathcal{W}_c(q, \mathbf{I}-\mathbf{P}\mathbf{P}^\dagger, (\mathbf{I}-\mathbf{P}\mathbf{P}^\dagger)^{-1}\mathbf{P}\tilde{\mathbf{T}}_{12}\mathbf{P}^\dagger)$. An integration of a function of the terms involved in (9) over the space of definite positive matrices permits to calculate the distribution of the term $\mathbf{R}\mathbf{R}^\dagger = \text{diag}(|r_1|^2, |r_2|^2, |r_3|^2)$ conditional on $\tilde{\mathbf{T}}_{22}$. A multiplication by the pdf of $\tilde{\mathbf{T}}_{22}$ and a last integration permits to express the joint pdf of the squared modulus of the sample matrix optimal coherence set as

$$p\left(\overline{\mathbf{R}}\right) = \frac{\tilde{\Gamma}_3(n)\pi^6}{\tilde{\Gamma}_3(n-3)\Gamma_3(3)^2}|\mathbf{I}-\overline{\mathbf{P}}|^n|\mathbf{I}-\overline{\mathbf{R}}|^{n-6} \\ {}_2\tilde{F}_1(n,n;3;\overline{\mathbf{P}},\overline{\mathbf{R}})\prod_{i<j}^{3}(|r_i|^2-|r_j|^2)^2 \quad (10)$$

where ${}_2\tilde{F}_1(.)$ represents the complex Gaussian hypergeometric function of matrix argument and $\overline{\mathbf{P}} \equiv \mathbf{P}\mathbf{P}^\dagger$, $\overline{\mathbf{R}} \equiv \mathbf{R}\mathbf{R}^\dagger$. By taking the log of 10 and removing terms that do not depend on $\mathbf{P}$, it is possible to define a pseudo-distance between a sample optimal coherence set $\overline{\mathbf{R}}$ and a given class one, $\overline{\mathbf{P}}_m$ as

$$d(\overline{\mathbf{R}}, \overline{\mathbf{P}}_m) = n\log|\overline{\mathbf{P}}_m - \mathbf{I}| - \log\ {}_2\tilde{F}_1(n,n;3;\overline{\mathbf{P}}_m,\overline{\mathbf{R}}) \quad (11)$$

For a large number of looks, it is possible to expand the hypergeometric function and then significantly simplify the expression of (11) [5].

3 Unsupervised Forest Classification

Unsupervised forest classification algorithms are applied to POL-inSAR data sets acquired in reapeat-pass mode by the DLR airborne E-SAR sensor at L band over the Traunstein scene (Germany). This test site is composed of various agricultural areas, forests and urban zones and is illustatred in **Figure 2**.

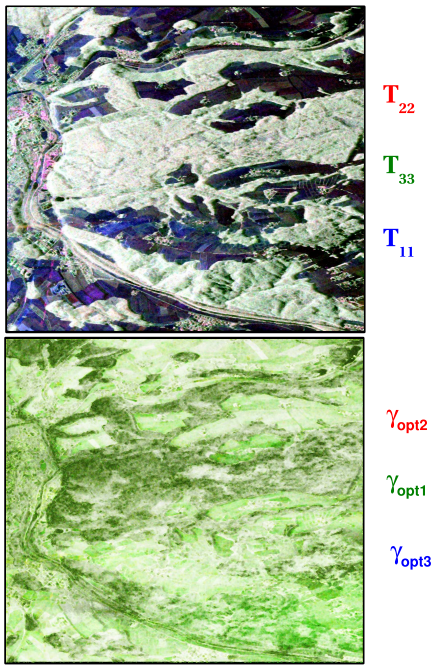

Figure 1: Color-coded POLSAR Pauli (top) and optimal coherence set (bottom) images

It can be observed that, in general, the polarimetric information shows a large contrats between vegetated and agricultural zones, whereas forested regions are characterized by an apparently uniform behavior. Oppositely, the optimal coherence set describes in a much more detailled way the structure of forested areas but may show similar very coherent features over low density forests and agricultural fields.

3.1 Unsupervised forest mapping

The proposed forest mapping algorithm relies on an identification of polarimetric basic scattering mechanisms. An unsupervised POLSAR segmentation provides clusters of polarimetrically compact pixels that are then analyzed using some of the H-A-$\underline{\alpha}$ decomposition parameters. A decision, adapted to the distribution of orthogonal scattering contributions, permits to classify the scene into three canonical mechanisms : Surface Reflection , Double bounce Reflexion and Volume Diffusion. The identification results displayed in **Figure 2** indicate a good correspondence between the VD class and the forest extent. Indeed, agricultural and forested areas are discriminated with a very good decision rate ($> 90\%$), but some errors can be noticed over built-up areas where some buildings and complex stuctures are assimilated to forest. Such artefacts are due to both an orientation related strong cross-polarized component and a high density of scatterers. This difficulty can be overcome using a Time-Frequency coherence analysis that discriminates coherent contributions from clutter.

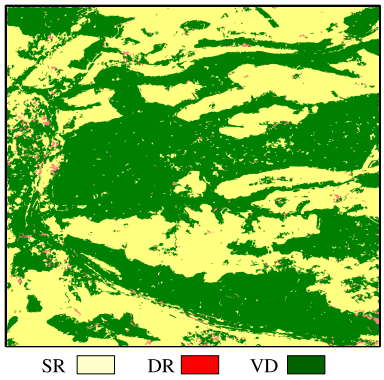

Figure 2: Identification of three basic scattering mechanisms

3.2 Unsupervised forest segmentation

Two POL-inSAR unsupervised segmentation procedures, based on (2) or on (11) are applied to data sets acquired with a 5m spatial baseline using a k-mean clustering algorithm. The segmentation is initialized using two indicators, A_1 and A_2, that were found to be relevant in [1] [2] for natural scene analysis. Arbitrary borders in the (A_1, A_2) permit to discriminate the number of relevant coherent scattering mechanisms. The color coding of the segmentation results shown in **Figure 3** is inspired from the optimal coherence image presented in **Figure 2**. Media with coherence properties that are independent of polarization are represented in white or light gray. A green color corresponds to a dominant first optimal coherence and relates a strong sensitivity on polarization. The segmented images show some similarities, particularly over areas with low or high correlation properties. For intermediate correlations, the classifier based on Wishart statistics tends to give homogeneous segments whereas the optimal coherence approach gives more heterogeneous features with sparse dark green clusters. A careful study of some available ground information revealed that the forest stands are indeed not as homogeneous as the Wishart segmentation results. This excessive smoothing is due to a range dependence of the backscattered power that can observed on the Pauli image in **Figure 3**. Particular external factors, incidence angle variations, due to topography or range position, are known to have a strong influence on classification results. The coherence is also affected in far range, but the influence on classification results is significantly less important.

3.3 Supervised forest classification

A comparative study showed that the class distribution in **Figure 3** and the forest stand biomass information had some common features. This potential relation is investigated using a supervised classification procedure. The measured biomass values (B) are gathered into three main classes : low (B<200), medium (200<B<310) and high (B>310) biomass in tons per hectare. Visual classification results are shown in **Figure 4**. The confusion matrices of both classification approaches are given in **Table 1** for the training set and in **Table 2** for the whole biomass map.

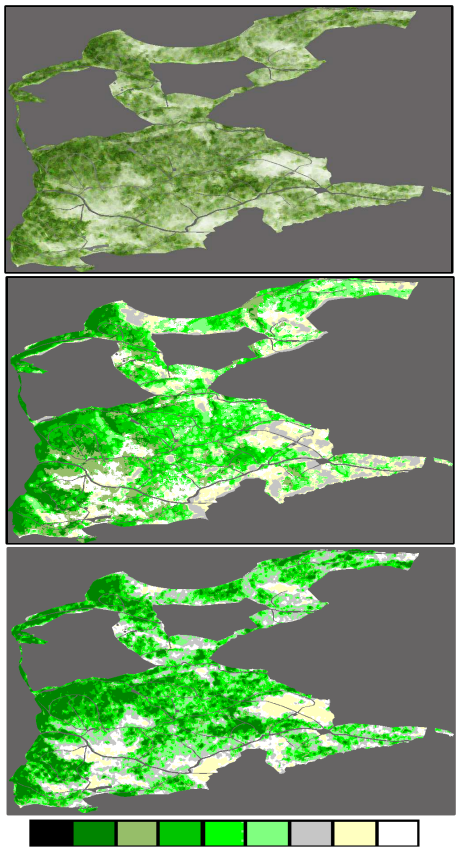

Figure 3: Color-coded POL-inSAR image (top) and unsupervised classification results using $\mathbf{T}_6$ (middle) and $|\gamma_{opti}|$ (bottom) statistics

The classification results indicate that both approaches give satisfying results over the low biomass class which is easily discriminated from denser media. For the high biomass class, the approach based on the optimal coherence set statistics performs around 15% better than the Wishart classification. This significant difference is due to misleading influence of the POLSAR information which varies with the incidence angle. This effect is particularly visible over the medium biomass class. The particularly good correct classification rate obtained with the Wishart approach is mainly due a dominant POLSAR influence on the statistical distance, i.e. the span information prevails over the coherent properties of the backscattered response. It is important to note that at far range the baseline decrease may also severely affect the classification performance.

3.4 Correction of coherence range dependence

The vegetation POL-inSAR coherence model presnetd in [3] relates coherence to the acquisition geometry, the volume properties and the ground to volume backscattered intensity ratio. Assuming a random volumetric response, the coherence polarimetric behavior is driven by the ground to volume ratio. Its estimation permits to compensate the range variations of some geometrical parameters, as shown in **Figure 5**.

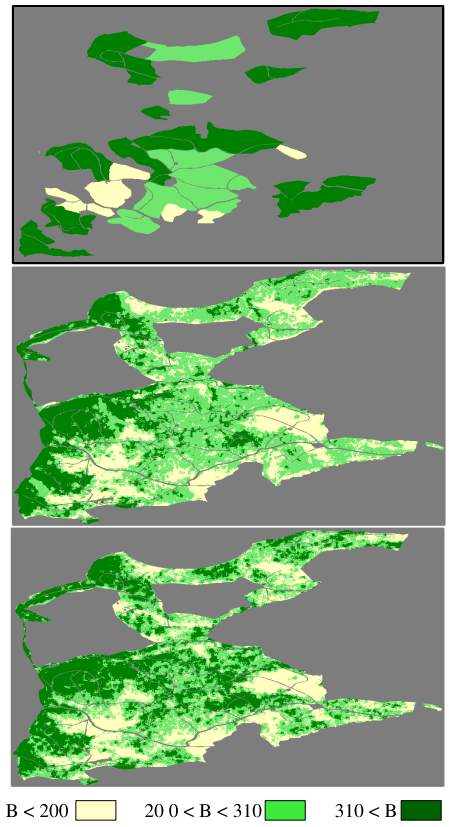

Figure 4: Biomass map (top) and supervised classification results using $\mathbf{T}_6$ (middle) and $|\gamma_{opti}|$ (bottom) statistics

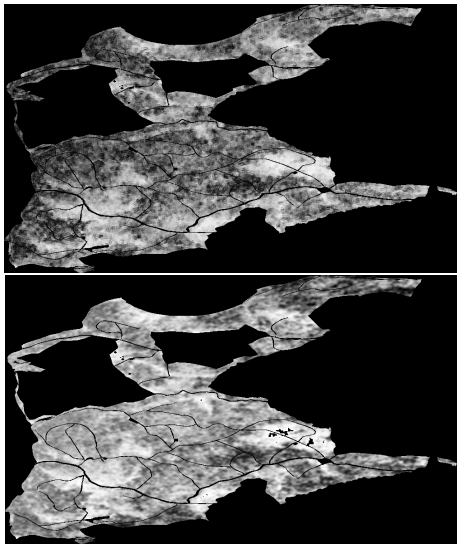

Figure 5: Original (top) and corrected (bottom) interferometric coherence in VV polarization

	using $\mathbf{T}_6$ statistics			using $\|\gamma_{opti}\|$ statistics		
	low	medium	high	low	medium	high
low	**78.3**	20	1.7	**78.5**	20	1.5
medium	14.6	**78.1**	7.3	17.9	**66.6**	15.5
high	0.9	4	**95.1**	0	6.1	**93.9**

Table 1: Training set confusion matrices (%)

	using $\mathbf{T}_6$ statistics			using $\|\gamma_{opti}\|$ statistics		
	low	medium	high	low	medium	high
low	**64.5**	28.2	7.3	**64.9**	29.6	5.5
medium	16.9	**70.2**	12.9	17.5	**56.3**	26.2
high	5.8	38	**56.2**	2.1	26.9	**71**

Table 2: Whole map confusion matrices (%)

4 Conclusion

In this paper, a new POL-inSAR classification method was introduced, based on the optimal coherence set statistics. It was shown that this information could successfully discriminate forest characteristics at L band and was less sensitive to perturbing factors due to strong invariance properties.

References

[1] L. Ferro-Famil, E. Pottier and J. S. Lee, "Unsupervised classification of natural scenes from polarimetric interferometric SAR data", in *Frontiers of remote sensing information processing*, C. H. Chen, Singapore : World Scientific Publishing, 2003, pp. 105-137.

[2] J.S. Lee, M.R. Grunes, T. Ainsworth , I. Hajnsek , T. Mette , and K.P. Papathanassiou, "Forest Classification based on L-Band Polarimetric and Interferometric SAR Data", *Proc. PolInSAR*, January 2005.

[3] K. P. Papathanassiou and S. R. Cloude, "Single-baseline polarimetric SAR interferometry", *IEEE Trans. Geosci. Remote Sensing*, vol. 39, no. 11, pp. 2352-2363, November 2001.

[4] L. Ferro-Famil, E. Pottier and J. S. Lee, "Unsupervised classification of multifrequency and fully polarimetric SAR images based on the H/A/Alpha-Wishart classifier", *IEEE Trans. Geosci. Remote Sensing*, vol. 39, no. 11, pp. 2332-2342, November 2001.

[5] R. J. Muirhead, *Aspects of Multivariate Statistical Theory*, Hoboke, NJ, USA : Wiley, 1982.